The importance of electron temperature in silicon-based terahertz quantum cascade lasers

L. Lever,* A. Valavanis, C. A. Evans, Z. Ikonić, and R. W. Kelsall
Institute of Microwaves and Photonics, School of Electronic and Electrical Engineering, University of Leeds, Leeds LS2 9JT, United Kingdom
(Dated: October 8, 2009)

Quantum cascade lasers (QCLs) are compact sources of coherent terahertz radiation. Although all existing QCLs use III–V compound semiconductors, silicon-based devices are highly desirable due to the high thermal conductivity and mature processing technology. We use a semi-classical rate-equation model to show that Ge/SiGe THz QCL active region gain is strongly enhanced by reducing the electron temperature. We present a bound-to-continuum QCL design employing L-valley intersubband transitions, using high Ge fraction barriers to reduce interface roughness scattering, and a low electric field to reduce the electron temperature. We predict a gain of $\sim 50\,\mathrm{cm}^{-1}$, which exceeds the calculated waveguide losses.

As silicon is the leading material for microelectronics, there has been great interest in developing silicon-based lasers. An electrically pumped Si-based laser could potentially be integrated with Si microelectronics, which would offer significant cost reduction over the III-V compounds used in existing semiconductor lasers.[1,2] To date, however, the indirect bandgap of group IV materials has frustrated all efforts to produce electrically pumped Si-based lasers. Quantum cascade lasers (QCLs) are intersubband devices, meaning that no change in electron wavevector occurs during the optical transition, and the indirect bandgap of Si is therefore no longer an obstacle.

Terahertz emission from III-V QCLs was first demonstrated in 2002,[3] but devices remain limited to cryogenic temperature operation (currently below $186\,\mathrm{K}$[4]) due to thermal back-filling of the lower radiative state from non-equilibrium LO-phonon distributions, and depopulation of the upper radiative state via LO-phonon emission.[5] Polar phonons are absent in group IV materials, and therefore higher operating temperatures may be possible, as well as emission within the Reststrahlen band of GaAs. Additionally, the increased intersubband lifetime may lead to narrower spectral linewidths.

Research towards silicon-based QCLs initially focused on p-type Si/SiGe heterostructures. This is primarily because the confinement effective mass of holes is smaller than that of electrons in the Δ-valleys of [100] silicon, and because control over p-type dopant placement is better than that of n-type dopants.[6] Mid-infrared electroluminescence from a p-type Si/SiGe heterostructure was first observed in 2000,[7] and subsequently in the THz frequency range in 2003.[8] However, lasing has not been observed in SiGe heterostuctures.

The valence subbands in SiGe heterostructures are highly non-parabolic, as there is considerable mixing of the light- and heavy-hole states. In contrast, the subbands in n-type systems are almost parabolic, which means that n-type intersubband devices are both simpler to design and should exhibit less inhomogeneous linewidth broadening. We have shown previously that [111] oriented n-type Si/SiGe heterostructures have potential for QCL development, in which system the quantization effective mass for electrons approximately equals that of holes in the [100] orientation.[9,10] However, issues with epitaxial growth on [111] wafers remain.

Recent progress in germanium epitaxy has allowed high quality $\mathrm{Ge/Si_{0.15}Ge_{0.85}}$ multiple quantum well heterostructures to be grown upon a virtual substrate, where the Ge fraction of the virtual substrate is chosen such that the heterostructure is strain-symmetrized to it.[11] Theoretical studies have shown that [100] Ge/SiGe heterostructures, in which the lowest energy conduction band valleys lie at the L-points, are very promising for QCL development, and device designs have been proposed.[12,13] In Ge, the longitudinal and transverse effective masses of the L-valleys are $m_l = 1.64m_e$ and $m_t = 0.08m_e$ respectively,[14,15] where m_e is the free electron rest mass. The quantization effective mass is given by $m_q = (3m_l m_t)/(2m_l + m_t) = 0.12m_e$,[16] which is approximately half that of heavy holes in SiGe quantum wells.[17] This allows wider heterolayers to be used, which simplifies epitaxial growth and increases the dipole matrix element for intersubband transitions.

In this work we demonstrate the use of a detailed rate-equation modeling tool to analyze the performance of Ge/SiGe QCLs and to identify viable device designs. We present a THz QCL design, using the $\mathrm{Ge/Si_{0.15}Ge_{0.85}}$ material system, which has lower barrier potential than earlier designs,[12] and operates at a lower electric field. Taking the design from ref. 12 as a reference for comparison, we simulate the performance of our design, taking into account the effect of multiple elastic and inelastic scattering processes, space-charge distribution and carrier heating. We show that the reduced interface roughness scattering rates and lower electric field in our design results in a decrease of the electron temperature, and offers a substantial improvement in active region gain.

Our device employs a bound-to-continuum scheme, with layer widths (starting from the injection barrier) of **3.7**, 5.8, **1.0**, 14.6, **1.4**, 12.3, **1.6**, 9.9, **1.9**, 8.3, **2.4**, 7.8, **2.9**, 7.6 nm, where bold text indicates $\mathrm{Si_{0.15}Ge_{0.85}}$ barriers and normal-weighted text indicates Ge wells. Underlined text indicates layers with a doping density of $2 \times 10^{16}\,\mathrm{cm}^{-3}$, providing a sheet doping den-

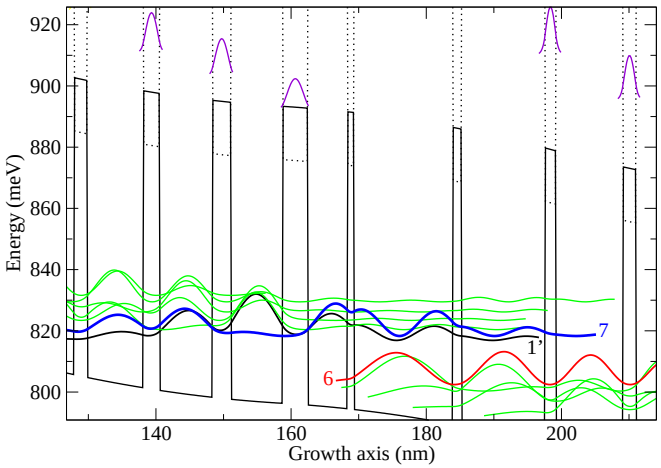

FIG. 1: Electron probability distributions under the design bias of 3.6 kV/cm. The L-valleys conduction band edge is shown as the solid black line, and the Δ-valley band edge as the dotted line. The lower energy states shown towards the bottom of the figure are the L-valley states, and the Δ-valley states are ~ 100 meV higher in energy. State 1' is the injector state, and the radiative transition is $7 \rightarrow 6$.

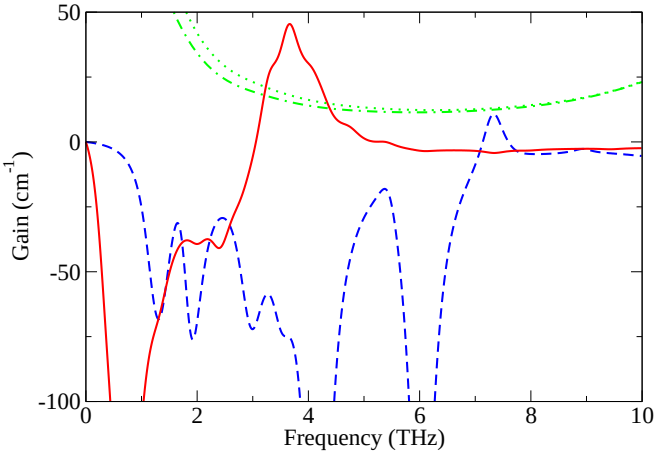

FIG. 2: Simulated gain at 4 K for our device (solid curve) and for the reference device designed by Driscoll *et al.* (dashed curve). Overlaid are the frequency-dependent waveguide losses (or equivalently, threshold gain) calculated for a metal-metal waveguide. The dotted curve is the loss for our device and the dot-dashed curve is for the reference; the two differ slightly as the average Ge content and doping density is different in the two devices.

sity of $8 \times 10^{10}\,\mathrm{cm}^{-2}$. Strain balance considerations require a $Si_{0.03}Ge_{0.97}$ virtual substrate.[18] Fig. 1 shows the squared magnitude of the envelope wavefunctions at the design bias of 3.6 kV/cm, calculated using an envelope function/one-band effective mass approximation, as described in ref. 10.

The conduction band profile of the L-valley system was calculated according to model-solid theory,[19] using the deformation potentials and valence band offsets determined by Rieger and Vogl.[14] The 4.2% mismatch in lattice constant between Si and Ge results in strain in the heterolayers. Hydrostatic strain shifts the conduction band edge as described in ref. 19. Owing to the symmetry of the system, uniaxial strain does not split the L-valley degeneracy. We calculate a conduction band offset of approximately 100 meV for the $Ge/Si_{0.15}Ge_{0.85}$ system, which provides sufficient confinement for optical transitions within the terahertz region.

In the L-valleys, the quantum wells are in the Ge layers and the barriers are in the SiGe layers, whereas for the Δ-valleys the quantum wells are in the SiGe and the barriers in the Ge layers. As the Δ-valley states are so much higher in energy than the L-valley states, we assume they are unpopulated. Furthermore, since they correspond to electronic states with different crystal momentum, the optical matrix elements with the L-valley confined states will be vanishingly small, and we can also neglect them in the calculation of the gain.

The state populations were determined by solving a set of rate equations,[20] accounting for electron scattering due to alloy disorder,[21] ionized impurities,[21] phonon deformation potentials,[22] interface roughness,[23] and carrier–carrier interactions.[18] The resulting charge density was used to calculate the internal electric fields by solving Poisson's equation, and Schrödinger's equation self-consistently.[24] The rate equations were then resolved, and the whole process iterated to convergence, with a self-consistent calculation of the electron temperature using an energy balance approach.[25]

Gain and current density were calculated using the subband populations obtained from the solutions of the rate equations.[24] In the optical gain calculations we assume Lorentzian lineshapes, with a full-width at half maximum (FWHM) of 2 meV. This is consistent with similar approaches in the simulation of GaAs/AlGaAs THz QCLs,[26] and experimental determination of the linewidth in THz QCLs.[3] Gain spectra for both our device and the reference structure at their respective design biases are shown in Fig. 2, together with waveguide losses, which were calculated using a transfer matrix method,[27] where the complex refractive indexes were calculated using the Drude model. We modeled a Cu-Cu waveguide,[28] with a 10-μm-thick active region sandwiched between two 20-nm-thick SiGe contact layers of the same composition as the virtual substrate, and doped at $1 \times 10^{19}\,\mathrm{cm}^{-3}$. The simulated gain in our device exceeds the waveguide losses by a factor of approximately two, whereas the gain for the reference device does not exceed the losses.

There are two principal reasons for the improved simulated performance of our device. Firstly, the photon energy in the reference device is larger than the intervalley phonon energy, which results in a reduction of the lifetime of the upper radiative state. The second reason relates to carrier heating due to elastic scattering processes, in particular interface roughness scattering. Owing to the requirement for energy conservation, if the destination subband is higher in energy than the initial subband,

only that fraction of the charge carriers with sufficient kinetic energy can participate in scattering. However, if the destination subband is lower in energy, all carriers can participate in scattering. As a consequence, elastic scattering processes tend to heat the electron distribution. Furthermore, increasing the applied electric field causes a larger separation between subbands and hence a higher electron temperature. In III-V THz QCLs at low lattice temperatures, LO-phonon emission cools the electron distribution. However, in non-polar materials, electron cooling only occurs via (much slower) phonon deformation potential scattering.

The fastest intersubband transitions in both designs are due to interface roughness scattering, even with the reduced $Si_{0.15}Ge_{0.85}$ barriers. For lattice temperatures below $\sim 50\,\mathrm{K}$, where the Bose-Einstein factor is much less than one, this leads to electron temperatures of $\sim 150\,\mathrm{K}$ in the reference design, and $\sim 100\,\mathrm{K}$ for our design. This reduction in the electron temperature leads to an increase in the intersubband lifetime of all the states, and an increase in the population inversion due to reduced thermal back-filling of the lower laser level.

We have developed a detailed rate-equation based model for Ge/SiGe QCLs, and have shown that higher electron temperatures can be expected in group IV QCLs than in III-V systems, owing to the lack of polar LO-phonon scattering. Using this model, we have developed a design for a bound-to-continuum Ge/SiGe THz QCL, and calculate gain at $\sim 3.5\,\mathrm{THz}$, with a threshold current density of $\sim 300\,\mathrm{A/cm^2}$. In order to reduce the electron temperature, we used high Ge-fraction barriers, reducing the interface roughness scattering rates, and a low electric field. We find a considerable increase in the lifetime of the upper radiative state in comparison to the existing design in the literature, and a four-fold improvement of the simulated material gain. Our calculations of the waveguide losses show that the simulated material gain is sufficient to expect lasing from this device.

* Electronic address: l.j.m.lever@leeds.ac.uk

[1] D. J. Paul, Semiconductor Science and Technology **19**, R75R108 (2004).
[2] L. Pavesi, *Towards the First Silicon Laser* (Kluwer Academic Publishers London, 2003).
[3] R. Köhler, A. Tredicucci, F. Beltram, H. E. Beere, E. H. Linfield, A. G. Davies, D. A. Ritchie, R. C. Iotti, and F. Rossi, Nature **417**, 156 (2002).
[4] S. Kumar, Q. Hu, and J. L. Reno, Applied Physics Letters **94**, 131105 (2009).
[5] B. S. Williams, Nature Photonics **1**, 517 (2007).
[6] R. W. Kelsall and R. A. Soref, International Journal of High Speed Electronic Systems **13**, 547 (2003).
[7] G. Dehlinger, L. Diehl, U. Gennser, J. Sigg, J. Faist, K. Ensslin, D. Grutzmacher, and E. Muller, Science **290**, 2277 (2000).
[8] R. Bates, S. A. Lynch, D. J. Paul, Z. Ikonić, R. W. Kelsall, P. Harrison, S. L. Liew, D. J. Norris, A. G. Cullis, W. R. Tribe, and D. D. Arnone, Applied Physics Letters **83**, 4092 (2003).
[9] L. Lever, A. Valavanis, Z. Ikonic, and R. W. Kelsall, Applied Physics Letters **92**, 021124 (2008).
[10] A. Valavanis, L. Lever, C. A. Evans, Z. Ikonic, and R. W. Kelsall, Physical Review B **78**, 035420 (2008).
[11] C. Lange, N. S. Köster, S. Chatterjee, H. Sigg, D. Chrastina, G. Isella, H. von Känel, M. Schäfer, M. Kira, and S. W. Koch, Phys. Rev. B **79**, 201306 (2009).
[12] K. Driscoll and R. Paiella, Applied Physics Letters **89**, 191110 (2006).
[13] K. Driscoll and R. Paiella, J. Appl. Phys. **102**, 093103 (2007).
[14] M. M. Rieger and P. Vogl, Physical Review B **48**, 14276 (1993).
[15] M. V. Fischetti and S. E. Laux, Journal of Applied Physics **80**, 2234 (1996).
[16] A. Rahman, M. S. Lundstrom, and A. W. Ghosh, Journal of Applied Physics **97**, 053702 (2005).
[17] M. Kahan, M. Chi, and L. Friedman, Journal of Applied Physics **75**, 8012 (1994).
[18] P. Harrison, *Quantum Wells, Wires and Dots: Theoretical and Computational Physics of Semiconductor Nanostructures* (Wiley, Chichester, 2005), 2nd ed.
[19] C. G. Van de Walle, Phys. Rev. B **39**, 1871 (1989).
[20] Z. Ikonic, P. Harrison, and R. W. Kelsall, Journal of Applied Physics **96**, 6803 (2004).
[21] T. Unuma, M. Yoshita, T. Noda, H. Sakaki, and H. Akiyama, Journal of Applied Physics **93**, 1586 (2003).
[22] M. Fischetti, Electron Devices, IEEE Transactions on **38**, 634 (1991).
[23] M. Califano, N. Q. Vinh, P. J. Phillips, Z. Ikonic, R. W. Kelsall, P. Harrison, C. R. Pidgeon, B. N. Murdin, D. J. Paul, P. Townsend, J. Zhang, I. M. Ross, and A. G. Cullis, Physical Review B **75**, 045338 (2007).
[24] V. D. Jovanovic, S. Hofling, D. Indjin, N. Vukmirovic, Z. Ikonic, P. Harrison, J. P. Reithmaier, and A. Forchel, Journal of Applied Physics **99**, 103106 (2006).
[25] P. Harrison, D. Indjin, and R. W. Kelsall, Journal of Applied Physics **92**, 6921 (2002).
[26] . D. Indjin, P. Harrison, R. W. Kelsall, and Z. Ikonic, IEEE Photonics Technology Letters **15**, 15 (2003).
[27] E. Anemogiannis, E. N. Glytsis, and T. K. Gaylord, J. Lightwave Technol. **17**, 929 (1999).
[28] M. A. Belkin, J. A. Fan, S. Hormoz, F. Capasso, S. P. Khanna, M. Lachab, A. G. Davies, and E. H. Linfield, Opt. Express **16**, 3242 (2008).